PROFESSOR XINYUE ZHANG (Orcid ID : 0000-0002-5027-6596)

Article type : Research Article

# Synthesis, Extracorporal Nephrotoxicity and 3D-QSAR of Andrographolide Derivatives

**Lili Gu[1], Qingqing Yu[2], Qin Li[1], Wenhai Huang[1], Ningzi Wu[1], Jiaqi Lu[1], Hong Lu[2], Xinyue Zhang[1*]**

[1]Key Laboratory of Neuropsychiatric Drug Research of Zhejiang Province, Hangzhou medical college, Hangzhou, 310013, China; 17826865042@163.com (G.L.); liqin@zjams.com.cn(L.Q.); cyj@zju.edu.cn(H.W.); wnzyky@126.com (W.N.); lujiaqi2018@sina.com(L.J.);

[2] College of Pharmaceutical science, Zhejiang Chinese Medical University, Hangzhou, 310053, PR China; m15757196155_2@163.com(Y,Q.); luhong@zcmu.edu.cn (L,H);

* Correspondence: zhangxy@zjams.com.cn; Tel.: +0571-8821-5600

**Abstract:** Andrographolide is a traditional Chinese medicine monomer with many pharmacological activities, but has potential nephrotoxicity. Here, we aim to investigate the relationship between modification of andrographolide structure and its nephrotoxicity. Twenty-three andrographolide derivatives were synthesized and their structures were confirmed by $^1$H-NMR and HRMS. Nephrotoxicity of these compounds against human renal tubular epithelial (HK-2) cells were evaluated using the MTT assay. The results indicated that most of them had significantly reduced nephrotoxicity, especially compounds **III**, **V**, **IX$_c$**, with $IC_{50}$ values of 1985, 1300, 806.9 μmol·L$^{-1}$, respectively, which were obviously superior to andrographolide ($IC_{50}$ 30.60 μmol·L$^{-1}$). However, compounds **I$_a$-I$_f$** ($IC_{50}$ values < 30 μmol·L$^{-1}$), the 14-OH derivatives of andrographolide, showed higher nephrotoxicity than that of andrographolide. Three dimensional quantitative structure-activity relationship (3D-QSAR) models of COMFA and

This article has been accepted for publication and undergone full peer review but has not been through the copyediting, typesetting, pagination and proofreading process, which may lead to differences between this version and the Version of Record. Please cite this article as doi: 10.1111/CBDD.13796

COMSIA were established (COMFA: $q^2 = 0.639$, $r^2 = 0.951$; COMSIA: $q^2 = 0.569$, $r^2 = 0.857$). This model allowed proposing five new compounds with lower theoretical nephrotoxicity, which would be worthwhile to synthesize and evaluate. We believe that predicted models will help us to understand the structural modification requirements of andrographolide to reduce the nephrotoxicity, and further investigations will be needed to determine the mechanism involved in the effect of less nephrotoxic compounds.

**Keywords:** andrographolide derivatives; nephrotoxicity; synthesis; 3D-QSAR

## 1. INTRODUCTION

Andrographolide ,a lactone diterpenoid compound, which can be isolated from traditional Chinese medicine (TCM) *Andrographis paniculata* (Burm. F.) Wall. Ex Nees (Family: Acanthaceae)(Islam, 2017), exhibits various biological activities such as anti-inflammatory (Li et al., 2017; W. Wang et al., 2019), antivirus (Paemanee, Hitakarun, Wintachai, Roytrakul, & Smith, 2019; Uttekar et al., 2012), anticancer (Peng et al., 2018; Reabroi et al., 2018; Wei, Zhang, & He, 2018), liver protection (Abdullah & Ismail, 2018), cardiovascular (Wu et al., 2018), neuroprotective effect (Tao et al., 2018), and is mainly used in clinic for treating cold, fever, gastroenteritis and upper respiratory tract. The nephrotoxicity of TCM has been reported since the 1980s (Upreti, Das, Kumar, Singh, & Khanna, 1989), and has attracted widespread attention (Feng, Fang, Gao, Liu, & Chen, 2018; Song, Y.Y., & Miao, 2018; Vanherweghem et al., 1993). The two androrapholide derivatives, andrographolide sodium bisulfite (Lianbizhi) and potassium dehydroandrograpolide succinate (Chuanhuning), were used for the treatment of pneumonia, bacillary dysentery and other diseases (Xu & Chen, 2014; Zhao & Cai, 2012). However it has been an increasing number of reports on their adverse reactions, particularly renal adverse reactions in clinic (Xiang et al., 2016; Yang et al., 2013). In the our previous studies, Lianbizhi and Chuanhuning injection had certain kidney damage effects in model of mice and rabbits, and the main injury site was the renal tubule (Lu, Zhang, Zhou, & Jin, 2010; Xing, Xu, & Lu, 2013). Further studies showed that Andro and its water soluble derivatives had a damage effect on human renal tubular epithelial (HK-2) cells (L.L. Gu, Xing, Wang, Zheng, & Lu, 2016; L. L. Gu, Zhang, Xing, Xu, & Lu, 2016; Lu et al., 2014).

Quantitative structure activity relationship (QSAR) analysis is an important computer simulation method (Neves et al., 2018; Potemkin, Potemkin, & Grishina, 2018), and is mainly used to study the relationship between compound structure and physicochemical properties or biological activity (Brahmbhatt, Molnar, Pavi, & Rastijac, 2018; Flores-Sumoza et al., 2018; Marquina et al., 2019; Toropov & Toropova, 2018). It was reported that QSAR was used to furnish relationship between molecular descriptors and the nitric oxide synthase inhibition activity, antiproliferative activity or alpha-glucosidase inhibiting activity in order to the search of more potent drugs in the andrographolide derivative family of compounds (A, Prasana, Muthu, Abraham, & David, 2019; Hazra et al., 2015; Moorthy, Ramos, & Fernandes, 2011). QSAR has also been widely used to study the relationship between compound structure and toxicity (Secretan et al., 2019; Shao, Hollert, Tarcai, Deutschmann, & Seiler, 2019). Among the QASR analysis

methods, comparative molecular field analysis (CoMFA) and comparative molecular similarity index analysis (CoMSIA) are the most commonly used (Chen et al., 2018; M. Wang et al., 2018).

Therefore, in this study, we focused on the relationship between modification of andrographolide structure and its nephrotoxicity. Firstly, a series of 23 andrographolide derivatives were synthesized..Then we used $^{1}$H-NMR and HRMS and the model of HK-2 cells to characterize all target compounds and their nephrotoxicity , respectively. QSAR models were constructed with CoMFA and CoMSIA to explore the relationship between structural changes and nephrotoxicity, which can be applied to predict the nephrotoxicity of andrographolide derivatives and provide a reference for the development of andrographolide drugs.

## 2. MATERIALS AND METHODS

### 2.1. General Information

Andrographolide (98.56%, TC) were provided by Shanxi YuNing Biotechnology Co., Ltd., (Shanxi, China), and all other chemicals and solvents were of analytical grade and purchased from commercial suppliers. Melting points were determined on the M-565 Melting-Point Apparatus (BUCHI Labortechnik AG, Switzerland). $^{1}$H-NMR spectra were recorded on ACF400 NMR spectrometer (Bruker Spectroscopic Instruments Co., Rheinstetten, Germany) with $CDCl_3$ as solvent. Coupling constants (J) and chemical shifts (δ) values were reported in hertz and ppm, respectively. High resolution mass spectra were carried out with Synapt G2 HDMS (Waters Co., America). Monitoring of the reactions was performed using silica gel TLC plates (Qingdao Haiyang Chemical Co., Ltd., Qingdao, China) and visualized under ZF-2 ultraviolet analyzer (Shanghai Anting electronic Instrument Factory, Shanghai, China) under light 254 nm. Column chromatography was performed on silica gel (200 to 300 mesh).

### 2.2. Chemistry

**2.2.1.** Procedure for the synthesis of Andrographolide 14-OH esterification derivatives ($I_{a-f}$)

Preparation of 3,19-isopropylidene andrographolide (1)

Following a literature method, andrographolide (7.0 g, 20 mmol), 4-toluenesulfonic acid pyridine salt (PPTS) (0.5 g, 2 mmol), 2,2-dimethoxypropane(18 mL) were added into dichloromethane (20 mL), and then the reaction mixture was stirred at 45 °C for 2h (the reaction progress was monitored by TLC with UV detection). The reaction mixture was evaporated under reduced pressure and washed with petroleum ether to give 3,19-isopropylidene andrographolide (**1**) crude product as a white solid. ESI-MS（m/z）:391.2 $[M+H]^+$.

Preparation of 14-OH esterification 3,19-isopropylidene andrographolide ($2_{a-f}$)

3,19-isopropylidene andrographolide (**1**, 0.39 g, 1 mmol), triethylamine (0.42 mL) were added into dichloromethane (15 mL) and chilled to 0 °C. A solution of DL-thioctic acid/ p-chlorobenzoyl chloride / pivaloyl chloride / acryloyl chloride / carbonochloridic acid / acetyl chloride (1 mmol) dissolved in dichloromethane (5 mL) was added dropwise, then the reaction mixture was moved to room temperature and stirred for 3-6h. The reaction

mixture was washed with saturation sodium bicarbonate and water, dried over $Na_2SO_4$, and concentrated in vacuo to get 14-OH esterification 3,19-isopropylidene andrographolide (**2a-f**) crude product.

Preparation of 14-OH esterification andrographolide ($I_{a-f}$)

Dilute acetic acid (1 mmol) were added into a solution of 14-OH esterification 3,19- isopropylidene andrographolide (**2a-f**) in THF (10 mL), and the reaction mixture was stirred at room temperature for 2 h. The reaction mixture was evaporated under reduced pressure and dissolved with ethyl acetate, washed with saturation sodium bicarbonate, water and saturation salt solution, successively, dried over $Na_2SO_4$, and concentrated in vacuo. The residue was purified by column chromatography using ethyl acetate/petroleum ether 2:1 to yield products $\mathbf{I_{a-f}}$.

14-DL-thioctic acid ester andrographolide ($I_a$)

Light yellow solid; 67% yield; m.p. 65.1-67.3 °C, $^1$H-NMR ($CDCl_3$, δ ppm): 7.04 (t, 1H) , 5.93 (d, J = 5.9 Hz, 1H), 4.88 (s, 1H), 4.88 (s, 1H), 4.50 (s, 1H), 4.23 (d, 1H), 4.16 (d, 1H), 3.55-3.44 (m, 2H), 3.33 (d, J = 10.7 Hz, 1H), 3.25-3.05 (m, 2H), 2.76(s, 3H), 2.41-2.31 (m, 6H), 1.97-1.80 (m, 6H), 1.68-1.60 (m, 5H), 1.46 (m, 2H), 1.40 –1.34 (m,1H), 1.25 (s, 4H), 0.67 (s , 3H). ESI-MS (m/z):561.2$[M+Na]^+$.

14-P-chlorobenzoyl acid ester andrographolide ($I_b$)

White solid; 59% yield; m.p. 98.5-100.9 °C, $^1$H-NMR ($CDCl_3$, δ ppm): 7.96 (d, J = 8.6 Hz, 2H), 7.45 (d, J = 8.6 Hz, 2H), 7.09 (t, J = 6.2 Hz, 1H), 6.17 (d, J = 5.8 Hz, 1H), 4.84 (s, 1H), 4.67-4.59 (m, 1H), 4.48 (s, 1H), 4.37 (d, J = 1.7 Hz, 1H), 4.13 (d, 1H), 3.77-3.66 (m, 1H), 3.47 (dd, J = 13.7, 5.2 Hz, 3H), 3.30 (d, J = 11.0 Hz, 1H), 2.62 -2.27 (m, 4H), 2.24-1.90 (m, 6H), 1.89-1.59 (m, 5H), 1.42-1.24 (m, 2H), 1.24 (s, 4H), 0.59 (s, 3H). ESI-MS(m/z): 511.2$[M+Na]^+$.

14-pivaloyl acid ester andrographolide ($I_c$)

Light yellow solid;71% yield;m.p. 157.8-158.6 °C, $^1$H-NMR ($CDCl_3$, δ ppm): 6.94 (t, J = 6.6Hz, 1H), 5.81 (d, J = 6.2 Hz, 1H), 4.82 (s, 1H), 4.54 (m, 1H), 4.42 (s, 1H), 4.14 (m, 1H), 4.07 (d, J = 11.2Hz, 1H), 3.48-3.35 (m, 3H), 3.25 (d, J = 11.2 Hz, 1H), 2.43-2.21 (m, 3H), 2.05-1.55 (m, 8H), 1.46-1.19 (m, 4H), 1.16 (s, 9H), 0.58 (s, 3H). ESI-MS (m/z): 457.3$[M+Na]^+$.

14-acryloyl acid ester andrographolide ($I_d$)

White solid;74% yield; m.p. 127.6-128.3 °C, $^1$H-NMR ($CDCl_3$, δ ppm): 7.03 (t, J = 5.9 Hz, 1H), 6.48 (dd, J = 17.3, 3.3 Hz, 1H), 6.15 (dd, J = 17.2, 10.4Hz, 1H), 6.01 (d, J = 5.2 Hz, 1H), 5.96 (d, J = 10.5 Hz, 1H), 4.86 (s, 1H), 4.59 (dd, J = 11.2, 6.2 Hz, 1H), 4.49 (s, 1H), 4.28 (d, J = 11.2 Hz, 1H), 4.17 (d, J = 11.0 Hz, 1H), 3.55–3.41 (m, 1H), 3.31 (d, J=11.0Hz,1H), 2.53–2.31 (m, 3H), 2.03–1.67 (m, 6H), 1.44–1.06 (m, 7H), 0.65 (s,3H). ESI-MS (m/z): 427.2$[M+Na]^+$.

14-carbonochloridic acid ester andrographolide ($I_e$)

Yellow solid;47% yield;m.p. 78.8-80.2 °C, $^1$H-NMR ($CDCl_3$, δ ppm): 7.07 (t, J = 6.6 Hz, 1H), 5.82 (d, J = 5.7 Hz, 1H), 4.82 (s, 1H), 4.60-4.54 (m, 1H), 4.51 (s, 1H), 4.24 (d, J = 9.4Hz, 2H), 4.20 (d, J = 2.6 Hz, 1H), 4.12 (d, J = 7.1 Hz, 1H), 3.48 (dd, J = 10.9, 4.7 Hz, 2H), 3.35 (d, J = 9.5 Hz, 1H), 3.29 (d, J = 21.5 Hz, 2H), 2.46- 2.27 (m, 6H), 1.64-1.42 (m, 3H), 1.34 (t, 3H), 1.25 (s, 4H), 0.67 (d, J = 8.0 Hz, 3H). ESI-MS (m/z):445.2$[M+H]^+$.

14-acetyl acid ester andrographolide ($I_f$)

White solid;57% yield;m.p. 170.3-172.5 °C, $^1$H-NMR ($CDCl_3$, δ ppm): 6.94 (t, J = 6.5 Hz, 1H), 5.85 (d, J = 5.7 Hz, 1H), 4.81 (s, 1H), 4.48 (m, J = 11.2 Hz, 1H), 4.43 (s, 1H), 4.18 (d, J = 1.2 Hz, 1H), 4.12 (d, J = 10.7 Hz, 1H), 3.49-3.36 (m, 1H), 3.26 (d, J = 10.6 Hz, 1H), 3.11(m，2H),2.55 (s, 2H), 2.06 (s, 3H), 2.35（m,3H）1.80 (m, 6H), 1.18 (s, 4H), 0.60 (s, 3H). ESI-MS (m/z): 415.2$[M+Na]^+$.

**2.2.2.** Procedure for the synthesis of andrographolide derivatives (II-IV)

Preparation of dehydrated andrographolide (II)

Andrographolide (17.5 g, 0.05 mol) was dissolved in pyridine (25 mL) at 100 °C and then succinic anhydride (5 g, 0.05 mol) was added. The reaction mixture was reflux and stirring at 105 °C for 2h. The reaction mixture was cooled and poured into 80 mL of water and stirring to crystallize. Placed for 6 h, washed the solid with water, dried over, purified by column chromatography using ethyl acetate/ petroleum ether 1:1 to yield products (**II**). White solid; 88% yield; m.p. 200.1-202.3 °C, $^1$H-NMR ($CDCl_3$, δ ppm): 7.11 (s, 1H), 6.80 (dd, J = 15.8, 10.1 Hz, 1H), 6.05 (d, J = 15.8 Hz, 1H), 4.75 (s, 2H), 4.71 (s, 1H), 4.46 (s, 1H), 4.15 (d, J = 11.1 Hz, 1H), 3.46–3.36 (m, 1H), 3.28 (d, J = 11.1 Hz, 1H), 2.39 (dd, J = 13.6, 1.4 Hz, 1H), 2.28-1.27 (m, 8H), 1.19 (s, 3H), 0.74 (s, 3H). ESI-MS (m/z): 332.2$[M+H]^+$.

Preparation of 19-O-succinate ester dehydrated andrographolide (III)

Dehydrated andrographolide (**II**, 0.332 g,1 mmol), succinic anhydride (0.202 g, 2 mmol), 4-dimethylarminopyridine (DMAP) were dissolved in dichloromethane (20 mL). Then, the whole solution was stirred under room temperature for 8 h. The reaction mixture was washed with water for several times firstly and saturation salt solution for three times seconrly, dried over, purified by column chromatography using ethyl acetate/ petroleum ether 5:1 to yield products (**III**). Yellow solid; 90% yield; m.p.132.1-133.7 °C, $^1$H-NMR ($CDCl_3$, δ ppm):7.17 (s, 1H), 6.88 (dd, J = 15.6, 10.0 Hz, 1H), 6.12 (d, J = 15.8 Hz, 1H), 4.81 (s, 2H), 4.55 (s, 1H), 4.42 (d, J = 11.6 Hz, 1H), 4.09 (d, J = 6.7 Hz, 1H), 3.72 (d, J = 7.0 Hz, 1H), 2.67-2.63(m, 2H), 2.33(d, J=10.0Hz,1H), 2.10–2.04(m, 2H), 1.77-1.39(m, 8H), 0.99(d, J= 6.7Hz, 3H), 0.84(s, 3H). ESI-MS (m/z):455.2$[M+Na]^+$.

Preparation of 3-O- chloroacetyl -19-O-(2-chloroacetyl)dehydrated andrographolide dehydrated andrographolide(3)

Dehydrated andrographolide (**II**, 0.664 g, 2 mmol), triethylamine(0.6 mL, 4.3 mmol), were dissolved in dichloromethane (15 mL) and chilled to 0 °C. Chloroacetyl chloride (0.33 mL, 4 mmol) was dissolved in dichloromethane (5 mL) added dropwise, and the reaction mixture was moved to room temperature stirred 1h. The reaction mixture was washed with water and saturation salt solution, concentrated in vacuo to get 3-O- chloroacetyl -19-O-(2-chloroacetyl) dehydrated andrographolide (**3**) crude product. ESI-MS (m/z):507.2 $[M+Na]^+$.

Preparation of andrographolide derivatives ($IV_{a-d}$)

3-O-chloroacetyl-19-O-(2-chloroacetyl) dehydrated andrographolide (**3**, 0.50 g, 1 mmol), diisopropylethylamine (0.60 mL, 3 mmol) were dissolved in tetrahydrofuran (10mL) and chilled to 0 °C. Morpholine/piperidine/pyrrolidine/ (4-hydroxypiperidino) acetyl was dissolved in tetrahydrofuran (10 mL) added dropwise, and the reaction mixture was moved to room temperature stirred 3-8 h. The reaction mixture was evaporated under reduced pressure and dissolved with ethyl acetate, washed with water and saturation salt solution, successively, dried over $Na_2SO_4$, purified by column chromatography using ethyl acetate / petroleum ether 10:1 to yield products $\mathbf{IV_{a-d}}$.

3-O-morpholinoacetyl-19-O-(2-morpholinoacetyl) dehydrated andrographolide (IVa)

Yellow solid; 77% yield ;m.p.121.7-123.5 °C, $^1$H-NMR ($CDCl_3$, δ ppm): 7.17 (s, 1H), 6.93 (dd, J = 15.7, 10.1 Hz, 1H), 6.14 (d, J = 15.8 Hz, 1H), 4.82 (s, 2H), 4.81 (s, 1H), 4.69 (dd, J = 10.5, 5.8 Hz, 1H), 4.57 (s, 1H), 4.37 (d, J = 11.8 Hz, 1H), 4.29 – 4.22 (m, 1H), 3.78 – 3.72 (m, 8H), 3.19 (s, 4H), 2.59 (d, J = 3.5 Hz, 8H), 2.11–1.40 (m, 6H), 1.37–1.12 (m, 4H), 1.01 (s, 3H), 0.90 (s, 3H). ESI-MS (m/z):587.3$[M+H]^+$.

3-O-piperidinoacetyl-19-O-(2-piperidinoacetyl) dehydrated andrographolide ($IV_b$)

Yellow solid; 80% yield; m.p.119.6-121.5 °C, $^1$H-NMR($CDCl_3$,δ ppm): 7.10 (s, 1H), 6.86 (dd, J = 15.7, 10.0 Hz, 1H), 6.06 (d, J = 15.8 Hz, 1H), 4.75 (s, 2H), 4.73 (s, 1H), 4.64 – 4.57 (m, 1H), 4.49 (s, 1H), 4.29 (d, J = 11.8 Hz, 1H), 4.17 (d, J = 11.8 Hz, 1H), 3.13 (d, J = 7.9 Hz, 4H), 2.44 (d, J = 26.6 Hz, 8H), 1.80–1.22 (m, 22H), 0.94 (s, 3H), 0.82 (s, 3H).ESI-MS(m/z):583.2$[M+H]^+$.

3-O-pyrrolidinoacetyl -19-O-(2-pyrrolidinoacetyl) dehydrated andrographolide ($IV_c$)

Yellow solid; 67%yield;m.p.127.8-129.1 °C,$^1$H-NMR($CDCl_3$,δ ppm):7.27(s,1H),6.13 (dd, J = 10.5, 4.4 Hz, 1H), 6.06 (d, J = 6.9 Hz, 1H), 4.83 – 4.74 (m, 2H), 4.68 (dd, J = 11.0, 4.9 Hz, 2H), 4.42 – 4.32 (m, 3H), 4.33 (d, J = 11.6 Hz, 1H), 4.29 – 4.19 (m, 2H), 4.18 – 4.00 (m, 1H), 3.33 (s, 4H), 2.66 (s, 8H), 1.82 (s,8H), 1.74 – 1.47 (m,6H), 1.01 (s, 3H), 0.80 (s, 3H). ESI-MS (m/z):555.3$[M+H]^+$.

3-O-(4-hydroxypiperidino) acetyl-19-O-[2-(4-hydroxypiperidino) acetyl] dehydrated andrographolide ($IV_d$)

Yellow solid; 60%yield;m.p.107.2-108.8 °C, $^1$H-NMR ($CDCl_3$,δ ppm): 7.17 (s, J = 1.9 Hz, 1H), 6.98 – 6.87 (dd, 1H), 6.16 (d J = 24.5Hz, 1H), 4.82 (d, J = 1.7 Hz, 2H), 4.81 (d, J = 1.3 Hz, 1H), 4.68 (dd, J = 10.7, 5.8 Hz, 1H), 4.56 (d, J = 1.2 Hz, 1H), 4.37 (d, J = 11.8 Hz, 1H), 4.25 (d, J = 11.8 Hz,1H), 3.78 – 3.69 (m, 2H), 3.23 (s, 2H), 3.32(m,4H),2.31 ( m, 8H), 1.72 – 1.66 (m, 4H), 1.62 – 1.53 (m, 4H), 1.35-1.21(m,8H),1.01 (s, 3H), 0.89 (s, 3H).ESI-MS(m/z):615.3$[M+H]^+$.

**2.2.3.** Procedure for the synthesis of Andrographolide derivatives (V-IX)

Preparation of 19-O- triphenylmethyl dehydrated andrographolide (4)

Dehydrated andrographolide (**II**, 2 g, 6 mmol), 4-nethylmorpholine (0.76 ml, 6.9 mmol) were dissolved in dichloromethane (20 mL). A solution of trityl chloride (1.7 g, 7.8 mmol) was dissolved in dichloromethane (10 mL) was added dropwise, ang then the reaction was stirred overnight. The reaction mixture was washed with water and saturation sodium bicarbonate, dried over $Na_2SO_4$, purified by column chromatography using ethyl acetate / petroleum ether 1:2 to yield products (**5**). ESI-MS（m/z）:575.2 $[M+H]^+$.

Preparation of 3-O-succinate ester 19-O- triphenylmethyl dehydrated andrographolide (5)

19-O-triphenylmethyl dehydrated andrographolide (**4**, 0.610 g, 1 mmol), succinic anhydride (0.101 g, 1 mmol), 4-dimethylarminopyridine (DMAP) were dissolved in dichloromethane (20 mL). Then, the whole solution was heated to reflux for 24h. After cooling the reaction mixture was washed with water and saturation salt solution, dried over $Na_2SO_4$, and concentrated in vacuo to get 3-O-succinate ester 19-O- triphenylmethyl dehydrated andrographolide (**5**) crude product.

Preparation of 3-O-succinate ester dehydrated andrographolide (V)

3-O-succinate ester 19-O-triphenylmethyl dehydrated andrographolide (**5**, 0.35 g, 0.5 mmol) was dissolved in dichloromethane (10 mL) and then formic acid was added to the reaction. Then the reaction mixture was stirred under room temperature for 2h, washed with saturation sodium bicarbonate, water and saturation salt solution, successively, dried over $Na_2SO_4$, purified by column chromatography using ethyl acetate / petroleum ether 2:1 to yield products (**V**). White solid; 63% yield; m.p. 121.7-123.3 °C, $^1$H-NMR ($CDCl_3$, δ ppm): 7.66 (s, 1H), 6.77 (dd, J = 15.8, 10.1 Hz, 1H), 6.15 (d, 1H), 4.89 (s, 2H), 4.50 (dd, J = 12.0, 4.1 Hz, 1H), 4.43 (s, 1H), 4.17 – 3.99 (d, 1H), 3.54 (d, J = 11.4 Hz, 1H), 2.46 (t, 2H), 2.36 (d, J = 12.6 Hz, 1H), 2.00 – 1.90 (t,2H),1.60–1.17 (m, 8H), 0.92 (s, 3H),0.86(s,3H). ESI-MS (m/z):455.2 $[M+Na]^+$.

Preparation of 3-O- acetyl-19-O- triphenylmethyl dehydrated andrographolide (6)

Acetic anhydride (1.98 mL, 2.1), 19-O-triphenylmethyl dehydrated andrographolide (**4**,0.6 g, 1.05 mmol), dimethylpyridine (0.112 g,1 mmol) were dissolved in dichloromethane (25 mL) and chilled to 0 °C. 1-ethylene-(3-dimethylaminopropyl) carbodiimide hydrochloride (EDC. HCl, 0.4 g, 2.1 mmol) was dissolved in dichloromethane (15 mL) added dropwise, and the reaction mixture was moved to room temperature stirred overnight. The reaction mixture was washed with saturation sodium bicarbonate, water and saturation salt solution, successively, dried over $Na_2SO_4$, purified by column chromatography using ethyl acetate / petroleum ether 1:2 to yield products (**6**). ESI-MS (m/z): 639.2 $[M+Na]^+$.

Preparation of 3-O- acetyl dehydrated andrographolide (VI)

3-O- acetyl-19-O- triphenylmethyl dehydrated andrographolide (**6**, 0.62 g, 1 mmol) was dissolved in dichloromethane (10 mL), formic acid (2 mL) was added to the reaction, and the reaction mixture was stirred under room temperature for 2h. The reaction mixture was washed with saturation sodium bicarbonate, water and saturation salt solution, successively, dried over $Na_2SO_4$, purified by column chromatography using ethyl acetate / petroleum

ether 1:2 to yield products (**VI**). White solid; 87% yield; m.p. 103.7-106.3 °C, $^1$H-NMR ($CDCl_3$, δ ppm): 7.17 (s, 1H), 6.89 (dd, J = 15.8, 9.7 Hz, 1H), 6.12 (d, J = 15.8 Hz, 1H), 4.81 (s, 2H), 4.80 (s, 1H), 4.67 (dd, J = 11.6, 4.6 Hz, 1H), 4.55 (s, 1H), 4.35 (d, J = 11.7 Hz, 1H), 4.17 (d, 1H), 2.06 (s,3H), 1.77 – 1.49 (m, 8H), 0.97 (s, 3H), 0.78 (s, 3H).ESI-MS (m/z): 397.2$[M+Na]^+$.

Preparation of 3-O- acetyl-19-O-(2-chloroacetyl) dehydrated andrographolide(7)

3-O- acetyl dehydrated andrographolide (**VI**, 0.62 g, 1 mmol), triethylamine (0.6mL, 4.3mmol), were dissolved in dichloromethane (10 mL) and chilled to 0 °C. Chloroacetyl chloride (0.33 mL, 4 mmol) was dissolved in dichloromethane (5mL) added dropwise, and the reaction mixture was moved to room temperature stirred 2h. The reaction mixture was washed with water and saturation salt solution, dried over $Na_2SO_4$, and concentrated in vacuo to get 3-O-acetyl-19-O-(2-chloroacetyl) dehydrated andrographolide (**7**) crude product.

Preparation of andrographolide derivatives ($VII_{a-d}$)

3-O-acetyl-19-O-(2-chloroacetyl) dehydrated andrographolide (**7**, 0.54 g, 1.23 mmol), diisopropylethylamine (0.64 mL, 3.69 mmol) were dissolved in tetrahydrofuran (10mL) and chilled to 0 °C. Morpholine/piperidine/pyrrolidine/ (4-hydroxypiperidino) acetyl was dissolved in tetrahydrofuran (10 mL) added dropwise, and the reaction mixture was moved to room temperature stirred 3-8 h. The reaction mixture was evaporated under reduced pressure and dissolved with ethyl acetate, washed with water and saturation salt solution, successively, dried over $Na_2SO_4$, purified by column chromatography using ethyl acetate / petroleum ether 2:1 to yield products**$VII_{a-d}$**.

3-O-acetyl-19-O-(2-morpholinoacetyl) dehydrated andrographolide ($VII_a$)

Light yellow solid; 73% yield; m.p. 113.7-115.3 °C, $^1$H-NMR ($CDCl_3$, δ ppm): 7.17 (s, 1H), 6.94 (dd, J = 15.7, 10.1 Hz, 1H), 6.14 (d, J = 15.7 Hz, 1H), 4.82 (s, 2H), 4.61 (s,1H), 4.57 (s, 1H), 4.43 (dd, J = 11.8,4.5 Hz, 1H), 4.28 (d, J = 11.6 Hz, 1H), 4.12 (d, J = 14.3Hz, 1H), 3.83 (t, 4H), 3.28 (s, 2H), 2.66-2.15 (t, 4H), 2.05 (s, 3H), 2.05-1.32(m,8H),1.03 (s, 3H), 0.89 (s, 3H).ESI-MS (m/z): 502.2$[M+H]^+$.

3-O-acetyl-19-O-(2-piperidinoacetyl) dehydrated andrographolide ($VII_b$)

Yellow solid; 60% yield; m.p. 139.2-141.6 °C, $^1$H-NMR ($CDCl_3$, δ ppm):. 7.16 (s, 1H), 6.93 (dd, J = 15.8, 10.1 Hz, 1H), 6.13 (d, J = 15.8 Hz, 1H), 4.81 (s, 2H), 4.61 ( s, 1H), 4.56 (s, 1H), 4.42 (dd, J = 11.7,4.4 Hz, 1H), 4.24 (d, J = 17.1Hz, 1H), 3.41 (s, 2H), 2.51 ( m, 4H), 2.04 (s, 3H), 1.72-1.22 (m, 14H), 1.03 (s, 3H), 0.89 (s, 3H).ESI-MS (m/z): 500.3$[M+H]^+$.

3-O-acetyl-19-O-(2-pyrrolidinoacetyl) dehydrated andrographolide ($VII_c$)

Yellow solid; 61% yield;m.p.123.8-125.1 °C, $^1$H-NMR ($CDCl_3$, δ ppm): 7.16 (s, 1H), 6.93 (dd, J = 15.8, 10.1 Hz, 1H), 6.13 (d, J = 15.8 Hz, 1H), 4.81 (s, 2H), 4.61 (dd, J = 9.4, 4.8 Hz, 1H), 4.56 (s, 1H), 4.42 (s, 1H), 4.26 (d, J = 11.8 Hz, 1H), 3.41 (s, 2H), 2.77 (t, 4H), 2.46 (d, J = 13.6 Hz, 1H), 2.04 (s, 3H), 1.94-1.79 (m, 4H), 1.72-1.29 (m, 8H), 1.03 (s, 3H), 0.89 (s, 3H).ESI-MS (m/z): 486.2$[M+H]^+$.

3-O-acetyl-19-O-[2-(4-hydroxypiperidino) acetyl] dehydrated andrographolide ($VII_d$)

Yellow solid; 65% yield;m.p.87.5-89.2 °C, $^1$H-NMR ($CDCl_3$, δ ppm): 7.17 (s, 1H), 6.93 (dd, J = 15.8, 10.1 Hz, 1H), 6.13 (d, J = 15.8 Hz, 1H), 4.81 (d, J = 1.4 Hz, 3H), 4.64-4.58 (m, 1H), 4.56 (s, 1H), 4.40 (d, J = 11.8 Hz, 1H), 4.24 (d, J = 11.8 Hz, 1H), 3.22 (d, J = 2.0 Hz, 2H), 2.88-2.83 (m, 1H), 2.51-2.31 (m, 4H), 2.04 (s, 3H), 2.00-1.90 (m, 2H), 1.88-1.32 (m, 10H), 1.02 (s, 3H), 0.89 (s, 2H).ESI-MS (m/z): 516.2$[M+H]^+$.

Preparation of 3-oxo-19-O- triphenylmethyl dehydrated andrographolide (8)

19-O-triphenylmethyl dehydrated andrographolide (**4**, 3 g, 5 mmol), was dissolved in dichloromethane (80 mL) and then pyridinum dichromate (4.3 g, 10 mmol) was added to the solution. The reaction mixture was refluxed for 48h. After cooling, the whole solution was filtered, and the filtrate was washed with water and saturation salt solution, dried over $Na_2SO_4$, and concentrated in vacuo to get 3-oxo-19-O- triphenylmethyl dehydrated andrographolide (**8**) crude product. ESI-MS (m/z): 573.2 $[M+H]^+$.

Preparation of andrographolide derivatives ($IX_{a-d}$)

The process of producing **VIII-IX$_{a-d}$** was similar to **VI-VII$_{a-d}$.**

3-oxo-dehydrated andrographolide (VIII)

White solid; 82% yield;m.p. 92.1-93.7 °C, 1H-NMR ($CDCl_3$, δ ppm): 7.19 (s, 1H), 6.94 (dd, J = 15.8, 10.1 Hz, 1H), 6.15 (d, J = 15.8 Hz, 1H), 4.85 (d, J = 1.5 Hz, 1H), 4.83 (s, 2H), 4.61 (s, 1H), 3.92 (d, J = 11.2 Hz, 1H), 3.54 (d, J = 11.2 Hz, 1H), 2.43 (d, J = 3.1 Hz, 1H), 2.16 – 1.47 (m, 8H), 1.23 (s, 3H), 1.01 (s, 3H).ESI-MS (m/z): 331.2$[M+H]^+$.

3-oxo-19-O-(2-morpholinoacetyl) dehydrated andrographolide ($IX_a$)

Yellow solid; 77% yield;m.p. 80.5-81.8 °C, $^1$H-NMR ($CDCl_3$, δ ppm): 7.18 (s, 1H), 6.97 (dd, J = 15.8, 10.1 Hz, 1H), 6.14 (d, J = 15.8 Hz, 1H), 4.83 (s, 2H), 4.72 (s, 1H), 4.63 (s, 1H), 4.58（d,J=11.3Hz,1H）3.98 (d, J = 11.3 Hz, 1H), 3.72 (t,J=4.5Hz, 4H), 3.16 (s, 2H), 2.78 (d, J = 14.9, 5.8 Hz, 1H), 2.47 (m, 4H), 2.14-1.36 (m, 8H), 1.18 (s, 3H), 1.14 (s, 3H). ESI-MS (m/z): 458.2$[M+H]^+$.

3-oxo-19-O-(2-piperidinoacetyl) dehydrated andrographolide ($IX_b$)

Yellow solid; 68% yield; m.p. 75.3-76.9 °C, $^1$H-NMR ($CDCl_3$, δ ppm): 7.12 (s, 1H), 6.90 (dd, J = 15.8, 10.1 Hz, 1H), 6.07 (d, J = 15.8 Hz, 1H), 4.76 (s, 2H), 4.62 (s, 1H), 4.56 (s, 1H), 3.91 (d, J = 11.3 Hz, 1H) , 3.06 (s, 2H), 2.41 (m, J = 5.3 Hz, 4H), 1.81 –1.50 (m, 8H), 1.47–1.20 (m, 4H), 1.11 (s, 3H), 1.07 (s, 3H). ESI-MS (m/z): 456.2$[M+H]^+$.

3-oxo-19-O-(2-pyrrolidinoacetyl) dehydrated andrographolide ($IX_c$)

Yellow solid; 71% yield; m.p. 71.2-73.1 °C, $^1$H-NMR ($CDCl_3$, δ ppm): 7.12 (s, 1H), 6.90 (dd, J = 15.7, 10.0 Hz, 1H), 6.09 (d, J = 13.0 Hz, 1H), 4.76 (s, 2H), 4.63 (s, 1H), 4.56 (d, J = 0.9 Hz, 1H), 4.35 (s, 1H), 3.93 (d, J = 11.3 Hz, 1H), 3.22 (s, 2H), 2.61 (m , 4H), 2.33 (d, J = 10.1 Hz, 1H), 2.27 – 1.75 (m, 8H), 1.69 – 1.58(m, 4H), 1.42-1.33(t,4H)1.11 (s, 3H), 1.07 (s, 3H). ESI-MS (m/z): 442.2$[M+H]^+$.

3-oxo-19-O-[2-(4-hydroxypiperidino) acetyl] dehydrated andrographolide ($IX_d$)

Yellow solid; 65% yield;m.p. 76.4-77.8 °C, $^1$H-NMR ($CDCl_3$, δ ppm): 7.12 (s, 1H), 6.90 (dd, J = 15.8, 10.1 Hz, 1H), 6.07 (d, J = 15.8 Hz, 1H), 4.90(s,2H),4.76 (s, J = 1.2 Hz, 1H), 4.64 (d, J = 11.3 Hz, 1H), 4.56 (s, 1H), 3.91 (d, J = 11.3 Hz, 1H), 3.70 – 3.60 (m, 1H), 3.12 (s, 2H), 2.81 – 2.63 (m, 4H), 2.44 (d, J = 10.8 Hz, 1H), 2.27 (m, 6.5 Hz, 4H), 1.81 – 1.42 (m, 8H), 1.11 (s, 3H), 1.07 (s, 3H). ESI-MS (m/z): 472.2$[M+H]^+$.

**2.3. Extracorporal nephrotoxicity assay**

HK-2 cells were purchased from Cell Center of the Chinese academy of medical sciences (Beijing, China), and the cells were previously derived from the ATCC. HK-2 cells were cultured in Dulbecco's Modified Eagle's Medium nutrient mixture F-12 (DMEM/F12 medium) supplemented with 10% fetal calf serum (FCS) at 37 °C in a humidified atmosphere of 5% $CO_2$ in air. The in vitro nephrotoxicity of andrographolide and all synthesized compounds was evaluated against HK-2 cells by MTT method. Different concentrations of drugs acted on cell for 24h. Then the optical density (OD) value was detected at wavelength of 490 nm using microplate reader iMark (Molecular Devices, LLC, Sunnyvale, CA, USA).. Cell survival rate (%) = (OD of administration group−OD of blank group)/(OD of control group−OD of blank group) × 100%. The value of inhibitory concentration 50 ($IC_{50}$) was calculated by GraphPad Prism 5 software (San Diego, CA, USA).

**2.4. QSAR study**

The QSAR model was constructed with SYBYL6.9 (Tripos Associates, St. Louis, MO, USA). The $IC_{50}$ for each compound was transformed into negative logarithm of $IC_{50}$ ($pIC_{50}$). The $pIC_{50}$ values were employed as dependent variable for the QSAR analysis. The molecular structures of synthesized compounds were generated and then divided into test (4 compounds) and training (20 compounds) datasets using a random selection method(J.T. & K., 2006). The training set is used to build the QSAR model, and the test set is used to evaluate the predictability of the generated models.

Molecules were digitized and optimized. Details are as follows: The compounds are transformed into 3D structures by Chem 3D software, and then imported into SYBYL-X software. Energy minimum of the compound molecules were set by Tripos force field, Gradient value as a standard termination is reduced to 0.005. If the calculation step difference is less than 0.005 for two consecutive times, the calculation is terminated, and the maximum repetition number (Max, Iterations) is increased to 1000. The molecular load type is Gasteiger-Huckel charge, and the rest parameters are kept as the default values of the software. Calculate and get the optimized molecules, which are saved as .mol2 file.

In this paper, the 14-acetyl acid ester andrographolide (compound $\mathbf{I_f}$)（**Figure 1**）, the most active molecule of the series with the lowest $IC_{50}$ value, was selected as the common scaffold for molecular alignment. All other synthesized compounds were aligned with the 14-acetyl acid ester andrographolide ($\mathbf{I_f}$). The comparative molecular field analysis (CoMFA) and comparative molecular similarity indices analysis (COMSIA) were used to get 3D-QSAR model. In CoMFA, the steric and electrostatic fields were calculated and in COMSIA steric, electrostatic, hydrophobic,

hydrogen-bond donor, hydrogen-bond acceptor fields were calculated. The relationship was quantified using partial least squares (PLS) with biological activity ($pIC_{50}$ value) as the dependent variable and CoMFA/CoMSIA descriptor as the independent variable. The cross-validation of the model was carried out using the leave-one-out method.

In order to improve the predicted quality of the model, conformational search method is used to select the compound molecular superposed conformation. According to the superposition of each molecule and template molecule, the new superposition conformation was selected and imported into the Training table. After refreshing the Training table, the steps of CoMFA and COMSIA were repeated, and finally get the 3D-QSAR model with reasonable cross-validation coefficient q2 value.

## 3. RESULTS AND DISCUSSION

### 3.1. Chemistry

The synthesis of andrographolide 14-OH esterification derivatives **($I_{a-f}$)** was outlined in Scheme 1. The first reaction of synthesizing **1** was followed as literature description (Jada et al., 2007), the second step was altered by adding the DL-thioctic acid, cathyl chloride and different acyl chloride. The final step of the reaction yielded the end product by deprotection under acidic conditions.

The synthesis of **II-IV** was outlined in Scheme 2. Andrographolide was dehydrated under alkaline conditions to form compound **II**. Target compound **III** was obtained from compound **II** through a one-step reaction with succinic anhydride. To get compound **$IV_{a-d}$**, firstly we used chloroacetyl chloride to connect to the two hydroxyl groups, then added different amines to the system.

The synthesis of **V-IX** was outlined in Scheme 3. The intermediate product **4** was synthesized through the reaction of dehydroandrographolide (**II**) with triphenylmethyl chloride. Target compound **5** was synthesized like **III**. Then removing protection under acidic conditions and getting the target compound **V**. We oxidized the hydroxyl group at position 3 to obtain compound **6** and **8**, then removed protection under acidic conditions, connected the hydroxyl group at position 19 with chloroacetyl chloride. Finally, the target compounds **$VII_{a-d}$** and **$IX_{a-d}$** were synthesized with different amines. The physical characteristics of target compounds were determined by $^1$H NMR and HRMS.

### 3.2. Extracorporal Nephrotoxicity

As shown in **Table 1**, MTT (3-(4, 5-dimethyl thiazolyl-2)-2, 5-diphenyltetrazolium bromide) assay was carried out in HK-2 cells after treatment for 24h, which revealed the nephrotoxicity of all the compounds. Exhilaratingly, most of the title compounds emerged less nephrotoxicity than andrographolide. The $IC_{50}$ of andrographolide 14-OH esterification derivatives (**$I_{a-f}$**) were less than that of andrographolide, suggesting that 14 hydroxyl esterification enhanced nephrotoxicity of andrographolide to some extent. Meanwhile our results showed that the nephrotoxicity of elimination of 14-OH derivatives were significantly reduced. The $IC_{50}$ of compound **II** was about 458.0 $\mu mol \cdot L^{-1}$ and obvious higher than andrographolide. On the basis of compound **II**, the nephrotoxicity of 3-OH acetylation derivatives (**VI**) was significantly reduced. Then connected 19-OH with different amine nephrotoxicity was increased. To the

contrary, oxidized 3-OH to the keto group, could reduce the nephrotoxicity, restructured 19-OH had no significant change in nephrotoxicity. 3-OH or 19-OH (**V**, **III**) connected with succinic anhydride nephrotoxicity had a large degree of change and $IC_{50}$ were up to 1300 and 1985 μmol·$L^{-1}$, respectively.

### 3.3. Statistical Analyses of CoMFA and CoMSIA Models

The COMFA and COMSIA models of 3D-QSAR were generation based on biological activity. The relevant results of the models were listed in **Table 2**. The cross-validation coefficient $q^2$ and the non-cross-validation coefficient $R^2$ represents the robustness and fitness of the model to reproduce the experimental value, and the value of criteria are $q^2$>0.5 and $R^2$>0.8.

The partial least square (PLS) results of the COMFA and COMSIA models were showed in **Table 2**. The optimal COMFA model yielded a $q^2$=0.639 with an optimal number of principal components (ONC) of 2, $R^2$=0.951, SEE=0.158 and F value of 163.747. The contribution of steric and electrostatic fields was 33.6% and 66.4%, respectively. The best COMSIA model yielded a $q^2$=0.569 with an ONC of 2, $R^2$ of 0.857, SEE=0.268 and F value of 51.096. The contribution of steric, electrostatic, hydrophobic, hydrogen-bond-donor and hydrogen-bond acceptor were 6.4%, 24.4%, 14.8%, 20.3% and 34.2%, respectively. Based on these field contributions, the electrostatic field was the most important field in the CoMFA model, whereas the hydrogen-bond acceptor field was the most important field in the CoMSIA model. All the parameters in the **Table 2** indicated that the CoMFA and CoMSIA models were robust and stable.

Further, based CoMFA and CoMSIA models were used to predict the activities of the training and test dataset compounds. The value of experimental versus predicted extracorporal nephrotoxicity for COMFA and COMSIA models were shown in **Table 3** and the scatter plots were illuminated in **Figure 2**. As shown in **Figure 2**, all points are situated around the diagonal lines, and there is no obvious deviated point present on them. The correlation coefficients $R^2$ of the COMFA and COMSIA models were 0.9506 and 0.8574, respectively. The $R^2$ of COMFA was higher than its COMSIA, which indicated COMFA model had higher predictive ability. In general, the models had a good correlation and further confirmed that COMFA and COMSIA models were predictive.

### 3.4 CoMFA Contour Maps

The COMFA and COMSIA contour with the template molecule $\mathbf{I_f}$ were generated. Those contours depicted default contribution levels. The COMFA steric and electrostatic contour maps were shown in **Figure 3**. The green contours indicated that introduction of bulky groups would increase activities, in contrast, the yellow patches illustrated where bulky groups addition would decrease activities（**Figure 3A**）. The blue contour in the COMFA electrostatic field indicates the electron-donating group, and the red contour represents that the electron-withdrawing group will be favorable to improve the activity.（**Figure 3B**）. It could be clearly seen in **Figure 3A** that there was a green patch at the position of 14-OH, indicating that introduce a large substitution group at this position would increase nephrotoxicity. Meanwhile there was a big yellow patch near 19-OH, that meaning that introduce bulky groups in this position would decrease nephrotoxicity. So the nephrotoxicity of the compounds $\mathbf{I_a}$-$\mathbf{I_f}$, which were

introduced a large substitution group at the position of 14-OH, were significantly higher than other compounds. In **Figure 3B**, there were two big blue patches near the position of 3-OH, which revealed that the regions with electron-withdrawing groups would increase the nephrotoxicity. Therefore the nephrotoxicity of the compounds $IX_a$-$IX_d$, which were formed by oxidation of 3-hydroxyl groups to acetyl groups and nitrogen-containing heterocyclic ligation with 19-OH were obviously reduced.

### 3.5 CoMSIA Contour Maps

The steric, electrostatic, hydrophobic and hydrogen bond acceptor contour maps of the COMSIA model were shown in **Figure 4**. The steric and electrostatic contour of COMSIA (**Figure 4A and 4B**) was in agreement well with that of COMFA.As shown in the COMSIA hydrophobic field (**Figure 4C**), yellow polyhedras meant that the regions with addition of hydrophobic groups would increase activity, white polyhedras meant that where introduction of hydrophilic groups would increase activities. There were large yellow polyhedra near the position of 3,19-OH, indicating that the nephrotoxicity of compound with hydrophobic group was higher, with hydrophilic groups was lower. So the nephrotoxicity of compound **III** and **V,** that hydrophilic carboxyl groups were introduced at 3 and 19-OH, respectively, were observably decreased. In the CoMSIA hydrogen bond acceptor field (**Figure 4D**), the magenta polyhedras showed that the regions with hydrogen-bond acceptor groups were beneficial for activity, while the red contour specifies the regions where hydrogen bond-accepting moiety may deteriorate the biological activity and hydrogen-bond donor groups was favorable for activity. Further, the hydrogen bond acceptor contour in **Figure 4D** corresponds to the electron-donating group in the electrostatic field contour map of **Figure 3B and 4B**.

### 3.6 Biological Activities Prediction of Newly Designed Compounds

The biological activities of newly designed compounds listed in **Table 4** were predicted using the best CoMFA and CoMSIA models. Before the activities' prediction, molecular alignment of the newly designed molecules was achieved using energy optimization and conformation search method. The predicted activities are reported in **Table 4**. The predicted nephrotoxicity of these newly designed compounds are lower than most of training dataset compounds. These results prove that generated 3D-QSAR models with significant predictive ability could be used for structural optimization of the newly designed compounds.

## 4. CONCLUSIONS

In this present study, twenty three of andrographolide derivatives were synthesized and the structures were confirmed by $^1$H-NMR and HRMS, then their nephrotoxicity against human proximal tubular HK-2 cell were evaluated. Most compounds exhibited lower nephrotoxicity than that of andrographolide, with compound **III** being the least active of the series and compound $\mathbf{I_f}$ being the most active. The conformation search-based alignment method with Gasteiger-Huckel charges yielded the best CoMFA and CoMSIA models. The contour maps suggest that the bulky hydrophilic group near the 19-OH position, the hydrophilic electron-donating groups near the 3-OH position and the lighter group near the 14-OH position will help to enhance the biological activities of this series of compounds. Based on contour maps information of the models, five new compounds were designed, and their biological activities were predicted. Hence, this work offered an important structural insight for design of

andrographolide derivatives with a lower nephrotoxicity, and further investigations will be needed to determine the mechanism involved in the effect of less nephrotoxic compounds.

**ACKNOWLEDGMENTS**

This study was supported by a grant from the Natural Science Foundation of Zhejiang province (LY18H280013), Chinese Medicine Reasearch Program of Zhejiang Province (2019ZQ004) and Key Laboratory of Neuropsychiatric Drug Research of Zhejiang Province (2019E10021).

**CONFILCT OF INTEREST**

The authors declare no conflict of interest.

**DATA AVAILABILITY STATEMENT**

The data that support the findings of this study are available from the corresponding author upon reasonable request.

## REFERENCES

A, S. B., Prasana, J. C., Muthu, S., Abraham, C. S., & David, H. A. (2019). Spectroscopic and quantum/classical mechanics based computational studies to compare the ability of Andrographolide and its derivative to inhibit Nitric Oxide Synthase. *Spectrochim Acta A Mol Biomol Spectrosc, 218*, 374-387. doi:10.1016/j.saa.2019.04.040

Abdullah, N. H., & Ismail, S. (2018). Inhibition of UGT2B7 Enzyme Activity in Human and Rat Liver Microsomes by Herbal Constituents. *Molecules : a journal of synthetic chemistry and natural product chemistry.*(10).

Brahmbhatt, H., Molnar, M., Pavi, V., & Rastijac, V. (2018). Synthesis, Characterization, Antibacterial and Antioxidant Potency of N-Substituted-2-Sulfanylidene-1,3-Thiazolidin-4-one Derivatives and QSAR Study. *Med Chem*. doi:10.2174/1573406415666181205163052

Chen, J., Chen, Y., Gan, X., Song, B., Hu, D., & Song, B. (2018). Synthesis, Nematicidal Evaluation, and 3D-QSAR Analysis of Novel 1,3,4-Oxadiazole-Cinnamic Acid Hybrids. *J Agric Food Chem, 66*(37), 9616-9623. doi:10.1021/acs.jafc.8b03020

Feng, X., Fang, S. N., Gao, Y. X., Liu, J. P., & Chen, W. (2018). Current research situation of nephrotoxicity of Chinese herbal medicin. *Chin J Chin Mater Med, 43*(03), 417-424.

Flores-Sumoza, M., Alcázar, J., Márquez, E., Mora, J., Lezama, J., & Puello, E. (2018). Classical QSAR and Docking Simulation of 4-Pyridone Derivatives for Their Antimalarial Activity. *Molecules : a journal of synthetic*

*chemistry and natural product chemistry., 23*(12).

Gu, L. L., Xing, W. M., Wang, Y. Q., Zheng, X. L., & Lu, H. (2016). Toxicity screening of andrographolide and its watersoluble derivatives on HK-2 cells and relative toxicity mechanism induced by andrographolide sodium bisulfite. *Chin J Pharmacol Toxicol, 30*(03), 229-235.

Gu, L. L., Zhang, X. Y., Xing, W. M., Xu, J. D., & Lu, H. (2016). Andrographolide-induced apoptosis in human renal tubular epithelial cells: Roles of endoplasmic reticulum stress and inflammatory response. *Environ Toxicol Pharmacol, 45*, 257-264. doi:10.1016/j.etap.2016.02.004

Hazra, A., Mondal, C., Chakraborty, D., Halder, A. K., Bharitkar, Y. P., Mondal, S. K., . . . Mondal, N. B. (2015). Towards the development of anticancer drugs from andrographolide: semisynthesis, bioevaluation, QSAR analysis and pharmacokinetic studies. *Curr Top Med Chem, 15*(11), 1013-1026. Retrieved from https://www.eurekaselect.com/129592/article

Islam, M. T. (2017). Andrographolide, a New Hope in the Prevention and Treatment of Metabolic Syndrome. *Front Pharmacol, 8*(23), 571-579. doi:10.3389/fphar.2017.00571

J.T., L., & K., R. (2006). On selection of training and test sets for the development of predictive QSAR models. *QSAR and Combinatorial Science, 25*(3).

Jada, S. R., Subur, G. S., Matthews, C., Hamzah, A. S., Lajis, N. H., Saad, M. S., . . . Stanslas, J. (2007). Semisynthesis and in vitro anticancer activities of andrographolide analogues. *Phytochemistry, 68*(6), 904-912. doi:10.1016/j.phytochem.2006.11.031

Li, Y., He, S., Tang, J., Ding, N., Chu, X., Cheng, L., . . . Wu, J. (2017). Andrographolide Inhibits Inflammatory Cytokines Secretion in LPS-Stimulated RAW264.7 Cells through Suppression of NF-kappaB/MAPK Signaling Pathway. *Evid Based Compl Alt, 2017*, 8248142. doi:10.1155/2017/8248142

Lu, H., Zhang, X. Y., Wang, Y. Q., Zheng, X. L., Zhao, Y., Xing, W. M., & Zhang, Q. (2014). Andrographolide sodium bisulfate-induced apoptosis and autophagy in human proximal tubular endothelial cells is a ROS-mediated pathway. *Environ Toxicol Pharmacol, 37*(2), 718-728. Retrieved from https://www.sciencedirect.com/science/article/pii/S1382668914000210?via%3Dihub

Lu, H., Zhang, X. Y., Zhou, Y. Q., & Jin, S. S. (2010). Toxic actions of andrographolide sodium bisulfite on kidneys of mice and rabbits. *Chin J Pharmacol Toxicol, 24*(03), 223-227.

Marquina, S., Maldonado-Santiago, M., Sánchez-Carranza, J. N., Antúnez-Mojica, M., González-Maya, L., Razo-Hernández, R. S., & Alvarez, L. (2019). Design, synthesis and QSAR study of 2'-hydroxy-4'-alkoxy chalcone derivatives that exert cytotoxic activity by the mitochondrial apoptotic pathway. *Bioorgan med chem*(1), 43-54.

Moorthy, N. S., Ramos, M. J., & Fernandes, P. A. (2011). Prediction of the relationship between the structural features of andrographolide derivatives and alpha-glucosidase inhibitory activity: a quantitative structure-activity relationship (QSAR) study. *J Enzyme Inhib Med Chem, 26*(1), 78-87. doi:10.3109/14756361003724760

Neves, B. J., Braga, R. C., Melo-Filho, C. C., Moreira-Filho, J. T., Muratov, E. N., & Andrade, C. H. (2018). QSAR-Based Virtual Screening: Advances and Applications in Drug Discovery. *Front Pharmacol, 9*, 1275. doi:10.3389/fphar.2018.01275

Paemanee, A., Hitakarun, A., Wintachai, P., Roytrakul, S., & Smith, D. R. (2019). A proteomic analysis of the anti-dengue virus activity of andrographolide. *Biomed Pharmacother, 109*, 322-332. doi:10.1016/j.biopha.2018.10.054

Peng, Y., Wang, Y., Tang, N., Sun, D. D., Lan, Y. L., Yu, Z. L., . . . C.Z., L. (2018). Andrographolide inhibits breast cancer through suppressing COX-2 expression and angiogenesis via inactivation of p300 signaling and VEGF pathway. *J exp clin canc res*(1), 248.

Potemkin, V., Potemkin, A., & Grishina, M. (2018). Internet Resources for Drug Discovery and Design. *Curr Top Med Chem, 18*(22), 1955-1975. doi:10.2174/1568026619666181129142127

Reabroi, S., Saeeng, R., Boonmuen, N., Kasemsuk, T., Saengsawang, W., Suksen, K., . . . Chairoungdua, A. (2018). The anti-cancer activity of an andrographolide analogue functions through a GSK-3beta-independent Wnt/beta-catenin signaling pathway in colorectal cancer cells. *Sci Rep, 8*(1), 7924. doi:10.1038/s41598-018-26278-8

Secretan, P. H., Karoui, M., Sadou-Yaye, H., Levi, Y., Tortolano, L., Solgadi, A., . . . Do, B. (2019). Imatinib: Major photocatalytic degradation pathways in aqueous media and the relative toxicity of its transformation products. *Sci Total Environ, 655*, 547-556. doi:10.1016/j.scitotenv.2018.11.270

Shao, Y., Hollert, H., Tarcai, Z., Deutschmann, B., & Seiler, T. B. (2019). Integrating bioassays, chemical analysis and in

silico techniques to identify genotoxicants in surface water. *Sci Total Environ, 650*(Pt 2), 3084-3092. doi:10.1016/j.scitotenv.2018.09.288

Song, Y. G., Y.Y., M., & Miao, M. S. (2018). Analysis on toxicity of traditional Chinese medicine containing aristolochic acid. *Chin J Tradit Chin Med Pharm, 33*(05), 1950-1954.

Tao, L., Zhang, L., Gao, R., Jiang, F., Cao, J., & Liu, H. (2018). Andrographolide Alleviates Acute Brain Injury in a Rat Model of Traumatic Brain Injury: Possible Involvement of Inflammatory Signaling. *Front Neurosci, 12*, 657. doi:10.3389/fnins.2018.00657

Toropov, A. A., & Toropova, A. P. (2018). Predicting Cytotoxicity of 2-Phenylindole Derivatives Against Breast Cancer Cells Using Index of Ideality of Correlation. *Anticancer res, 38*(11), 6189-6194. Retrieved from http://ar.iiarjournals.org/content/38/11/6189.full.pdf

Upreti, K. K., Das, M., Kumar, A., Singh, G. B., & Khanna, S. K. (1989). Biochemical toxicology of argemone oil. IV. Short-term oral feeding response in rats. *Toxicology, 58*(3), 285-298. doi:10.1016/0300-483x(89)90142-x

Uttekar, M. M., Das, T., Pawar, R. S., Bhandari, B., Menon, V., Nutan, . . . Bhat, S. V. (2012). Anti-HIV activity of semisynthetic derivatives of andrographolide and computational study of HIV-1 gp120 protein binding. *Eur J Med Chem, 56*, 368-374. doi:10.1016/j.ejmech.2012.07.030

Vanherweghem, J. L., Depierreux, M., Tielemans, C., Abramowicz, D., Dratwa, M., Jadoul, M., . . . et al. (1993). Rapidly progressive interstitial renal fibrosis in young women: association with slimming regimen including Chinese herbs. *Lancet, 341*(8842), 387-391. doi:10.1016/0140-6736(93)92984-2

Wang, M., Wang, Y., Kong, D., Jiang, H., Wang, J., & Cheng, M. (2018). In silico exploration of aryl sulfonamide analogs as voltage-gated sodium channel 1.7 inhibitors by using 3D-QSAR, molecular docking study, and molecular dynamics simulations. *Comput Biol Chem*, 214-225.

Wang, W., Wu, Y., Chen, X., Zhang, P., Li, H., & Chen, L. (2019). Synthesis of new ent-labdane diterpene derivatives from andrographolide and evaluation of their anti-inflammatory activities. *Eur J Med Chem, 162*, 70-79. doi:10.1016/j.ejmech.2018.11.002

Wei, R. J., Zhang, X. S., & He, D. L. (2018). Andrographolide sensitizes prostate cancer cells to TRAIL-induced apoptosis. *Asian J Androl, 20*(2), 200-204. doi:10.4103/aja.aja_30_17

Wu, T., Chen, X., Wang, Y., Xiao, H., Peng, Y., Lin, L., . . . Shuai, X. (2018). Aortic plaque-targeted andrographolide

delivery with oxidation-sensitive micelle effectively treats atherosclerosis via simultaneous ROS capture and anti-inflammation. *Nanomedicine, 14*(7), 2215-2226. doi:10.1016/j.nano.2018.06.010

Xiang, D., Wang, M. D., Wang, W. Q., Shi, C. Y., Xie, X. J., & Fang, J. G. (2016). Analysis and exploration on adverse reactions of four kinds of andrographolide injections. *Chin J Chin Mater Med, 41*(12), 2350-2355.

Xing, W. M., Xu, Z. L., & Lu, H. (2013). Preliminary study on the nephrotoxicity and its mechanism of Chuanhuning injection. *Chin J Exp Tradit Med, 19*(20), 263-267.

Xu, H., & Chen, F. G. (2014). Clinical observation of potassium dehydrographolide succinate injection in the treatment of viral pneumonia. *Chin Comm Doc, 30*(12), 92-93.

Yang, W. B., Wang, X. W., Yu, J. Y., Jing, Z. W., Wang, Z., Cao, J. L., & Jiang, F. (2013). Analysis of 253 Cases of ADR/AE Induced by Lianbizhi Injection. *Chin J Pharmacov, 10*(01), 46-50.

Zhao, X. Y., & Cai, X. H. (2012). Clinical application of Lianbizhi injection in pediatrics. *Mil Med J Southeast Chin, 14*(04), 359+378.

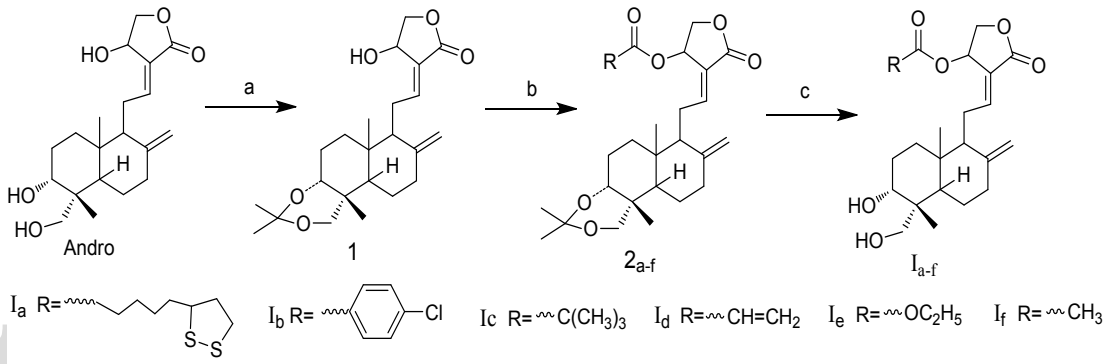


**Scheme 1.** Synthesis of andrographolide 14-OH esterification derivatives (**$I_{a-f}$**). Reagents and conditions: (a) $H_3CC(OCH_3)_2CH_3$, PPTS, $CH_2Cl_2$, reflux, 2h; (b) $NEt_3$, $CH_2Cl_2$, rt, RCOOH/ RCOCl /ClCOOEt, 2h; (c)AcOH:$H_2O$(7:3), 3h.

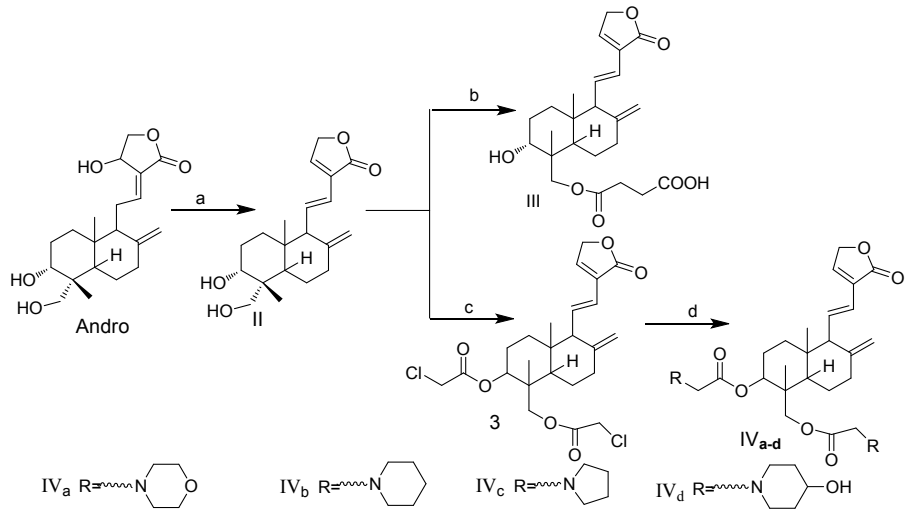


**Scheme 2.** Synthesis of target compounds **II-IV**. Reagents and conditions: (a) Succinic anhydride pyridine, refiux, 2h; (b) succinic anhydride, DMAP, $CH_2Cl_2$, 5h; (c) Chloroacetyl chloride, $Et_3N$, $CH_2Cl_2$, rt ,2h; (d) Amine, DIPEA, THF, rt, 3h.

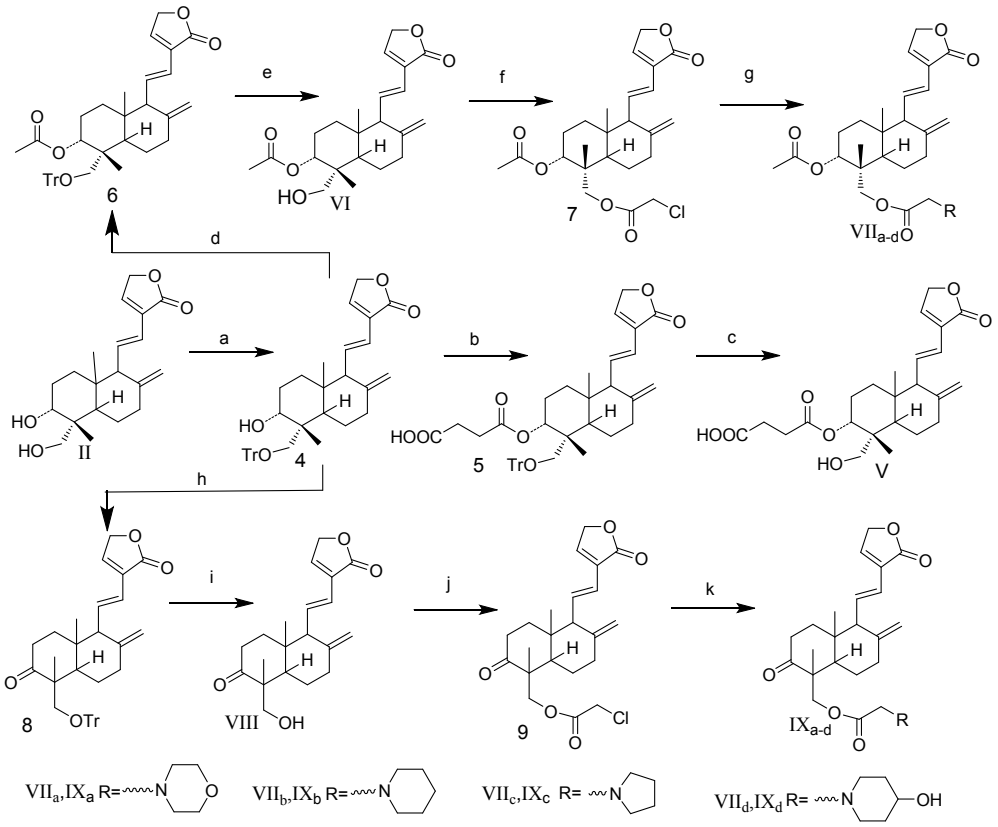


**Scheme 3.** Synthesis of target compounds **V-IX**. Reagents and conditions: (a) TrCl, N-methymorpholine, 24h; (b) succinic anhydride, DMAP, $CH_2Cl_2$, refiux, 24h; (c) HCOOH, $CH_2Cl_2$, rt, 2h; (d) $Ac_2O$, EDC, DMAP, $CH_2Cl_2$, rt, 12h; (e) HCOOH, $CH_2Cl_2$, rt, 2h; (f) Chloroacetyl chloride, $Et_3N$, $CH_2Cl_2$, rt, 2h; (g) Amine,

DIPEA, THF, rt, 2h; (h) PDC, $CH_2Cl_2$, reflux, 48h; (i) HCOOH, $CH_2Cl_2$, rt, 2h; (j) Chloroacetyl chloride, $Et_3N$, $CH_2Cl_2$, rt, 2h; (k) Amine, DIPEA, THF, rt, 2h.

**Table 1. The** $IC_{50}$ value of andrographolide and its derivatives (**I-IX**) in HK-2 cells.

| Compounds | $IC_{50}$/μmol·L$^{-1}$ | Compounds | $IC_{50}$/μmol·L$^{-1}$ |
|---|---|---|---|
| **Andrographolide** | 30.60 | **$IV_d$** | 338.7 |
| **$I_a$** | 20.63 | **V** | 1300 |
| **$I_b$** | 17.06 | **VI** | 685.0 |
| **$I_c$** | 28.66 | **$VII_a$** | 201.8 |
| **$I_d$** | 17.84 | **$VII_b$** | 114.0 |
| **$I_e$** | 25.60 | **$VII_c$** | 307.7 |
| **$I_f$** | 17.05 | **$VII_d$** | 162.3 |
| **II** | 458.0 | **VIII** | 757.1 |
| **III** | 1985 | **$IX_a$** | 786.6 |
| **$IV_a$** | 416.8 | **$IX_b$** | 460.0 |
| **$IV_b$** | 190 | **$IX_c$** | 806.9 |
| **$IV_c$** | 75.84 | **$IX_d$** | 622.0 |

**Table 2.** Summary of the results obtained from COMFA and COMSIA analyses.

| Parameter | CoMFA | COMSIA |
|---|---|---|
| $R^2$ (correlation coefficient squared) | 0.951 | 0.857 |
| ONC (the optimal number of components) | 2.000 | 2.000 |
| $q^2$ LOO (leave-one-out cross validation correlation coefficient squared) | 0.639 | 0.569 |
| F value | 163.747 | 51.096 |

| | | |
|---|---|---|
| SEE | 0.158 | 0.268 |
| Field distribution (%) | | |
| Steric | 33.6 | 6.4 |
| Electrostatic | 66.4 | 24.4 |
| Hydrophobic | - | 14.8 |
| Donor | - | 20.3 |
| Acceptor | - | 34.2 |

**Table 3.** .Experimental and predicted extracorporal nephrotoxicity ($pIC_{50}$) from 3D-QSAR of andrographolide and its derivatives.

| Compounds | Experimental $pIC_{50}$ | CoMFA | | CoMSIA | |
|---|---|---|---|---|---|
| | | Predicted $pIC_{50}$ | Residual | Predicted $pIC_{50}$ | Residual |
| **Andrographolide** | 4.51 | 4.477 | -0.03 | 4.526 | 0.016 |
| **$I_a$** | 4.69 | 4.794 | 0.104 | 4.763 | 0.073 |
| **$I_b$*** | 4.76 | 4.143 | -0.617 | 3.979 | -0.781 |
| **$I_c$*** | 4.54 | 4.471 | -0.069 | 4.144 | -0.396 |
| **$I_d$** | 4.75 | 4.490 | -0.26 | 4.449 | -0.301 |
| **$I_e$** | 4.59 | 4.780 | 0.190 | 4.662 | 0.072 |
| **$I_f$** | 4.77 | 4.535 | -0.235 | 4.694 | -0.076 |
| **II** | 3.34 | 3.186 | -0.154 | 3.591 | 0.251 |
| **III** | 2.70 | 2.851 | 0.151 | 2.997 | 0.297 |
| **$IV_a$** | 3.38 | 3.521 | 0.141 | 3.534 | 0.154 |
| **$IV_b$*** | 3.72 | 3.387 | -0.333 | 3.573 | -0.207 |
| **$IV_c$** | 4.12 | 3.833 | -0.287 | 3.200 | -0.920 |
| **$IV_d$** | 3.47 | 3.519 | 0.049 | 3.552 | 0.082 |
| **V** | 2.89 | 2.797 | -0.093 | 2.800 | -0.09 |
| **VI** | 3.16 | 3.257 | 0.097 | 3.189 | 0.029 |
| **$VII_a$** | 3.70 | 3.840 | 0.140 | 3.676 | -0.024 |
| **$VII_b$** | 3.94 | 4.011 | 0.071 | 3.889 | -0.051 |
| **$VII_c$*** | 3.51 | 3.718 | 0.208 | 3.149 | -0.361 |
| **$VII_d$** | 3.79 | 4.015 | 0.225 | 3.889 | 0.099 |

| | | | | | |
|---|---|---|---|---|---|
| **VIII** | 3.12 | 3.042 | -0.078 | 3.092 | -0.028 |
| **$IX_a$** | 3.10 | 3.104 | 0.004 | 3.274 | 0.174 |
| **$IX_b$** | 3.34 | 3.350 | 0.010 | 3.467 | 0.127 |
| **$IX_c$** | 3.09 | 3.041 | -0.049 | 3.068 | -0.022 |
| **$IX_d$** | 3.21 | 3.217 | 0.007 | 3.347 | 0.137 |

*Test set compounds: $pIC_{50} = -\log(IC_{50})$;

**Table 4**. Newly designed compounds structures with predicted biological activities.

| No. | Compound | Predicted $pIC_{50}$ | |
|---|---|---|---|
| | | CoMFA Model | CoMSIA Model |
| 1 | 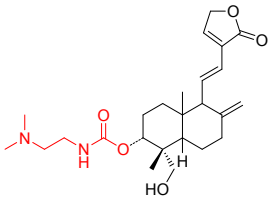 | 3.710 | 3.615 |
| 2 | 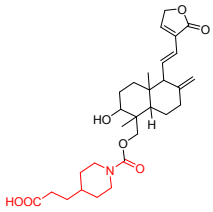 | 3.412 | 3.359 |

| | | | |
|---|---|---|---|
| 3 | 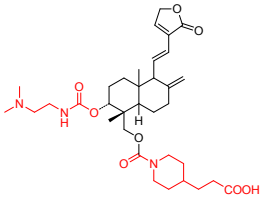 | 3.339 | 3.356 |
| 4 | 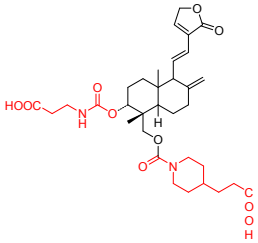 | 3.414 | 3.405 |
| 5 | 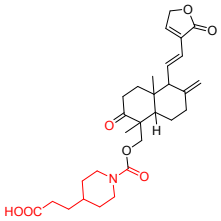 | 3.652 | 3.300 |

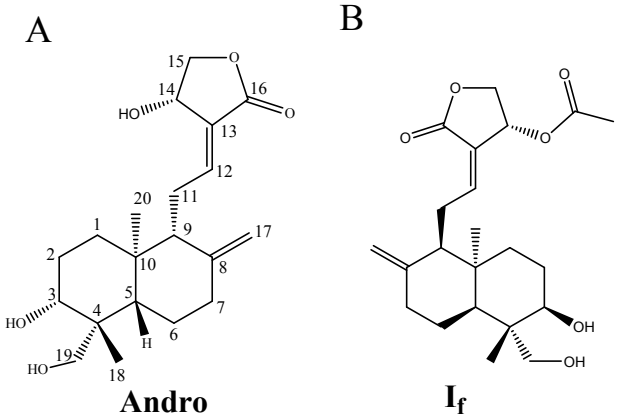


**Figure 1.** The structure of andrographolide (A) and compound $\mathbf{I_f}$ (B).

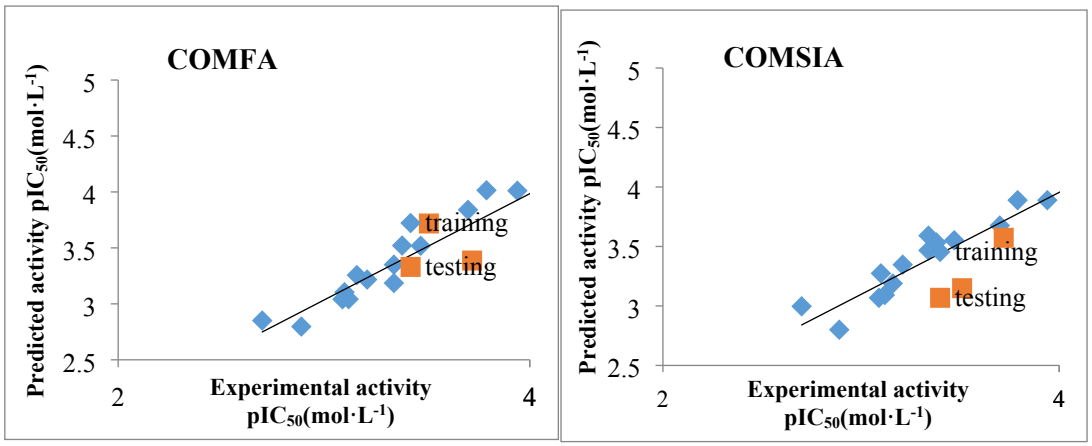


**Figure 2.** Plot of experimental and predicted $pIC_{50}$ for the COMFA and COMSIA models.

A B

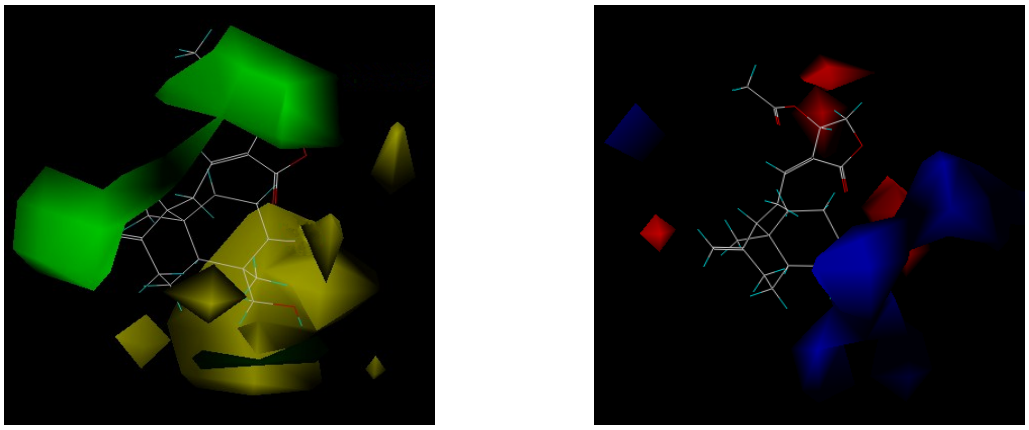

**Figure 3.** Space field(A) and static electric field(B) three-dimensional equipotential diagram of COMFA. The molecular structure is the template molecule compound If, the most active compound of the series.

A B

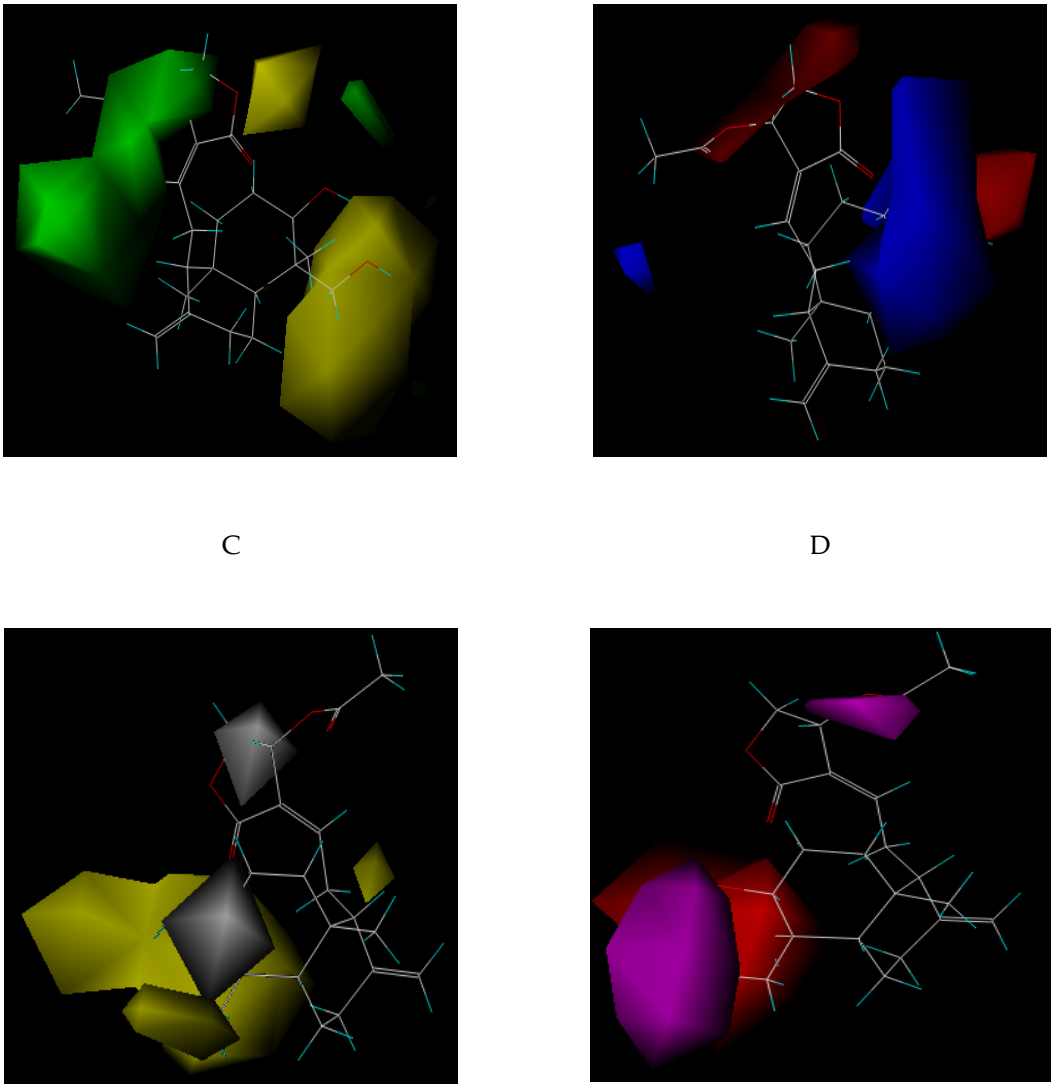


**Figure 4.** COMSIA contour maps of steric (A), electrostatic (B), hydrophobic(C), and H-bond acceptor fields(D). The molecular structure is the template molecule compound If, the most active compound of the series.